Field deployment and evaluation of a prototype autonomous two dimensional acoustic backscatter instrument: the Bedform And Suspended Sediment Imager (BASSI)

Benjamin D. Moate[1]*, Peter D. Thorne[1], and Richard D. Cooke[1]

1. National Oceanography Centre,

Joseph Proudman Building,

6, Brownlow Street,

Liverpool, L3 5DA, United Kingdom.

Corresponding authors. Email: bdmoate@gmail.com, pdt@noc.ac.uk

Abstract

The processes of sediment entrainment, transport and deposition over bedforms are highly dynamic and temporally and spatially variable. However, most measurements of these processes tend to be collected in a vertical line at one spatial location above the bed; one dimensional in the vertical, 1D-V. Such measurements capture the temporal signature, and, to a lesser degree, the spatial variability when bedforms migrate, and they have contributed greatly to our understanding of sediment transport processes. It is generally acknowledged, however, that such 1D-V systems provide a limited description of the spatially three dimensional processes occurring at the turbulent and intra-wave time scales. It would undoubtedly facilitate the interpretation of fundamental sediment processes above bedforms if other spatial dimensions could be simultaneously interrogated. To this end a multi-frequency acoustic array has been developed to measure suspended sediments and bedforms over a horizontal transect of the bed in the vertical, providing two dimensional observations in the vertical and horizontal, 2D-HV. This new acoustic instrument, the BASSI; Bedform And Suspended Sediment Imager, has been deployed in the River Dee tidal estuary in the UK. The design of the BASSI and results from the deployment are presented and its performance assessed against more conventional instrumentation. Measurements and images of 2D-HV suspended sediments and bedforms are provided to illustrate the capability and future use of the BASSI for the investigation of sediment transport processes.

1. Introduction

In energetic shallow marine waters, seabed sediments are easily entrained into suspension, with the subsequent transport and fate of such suspensions of critical interest in terms of morphodynamic evolution, changes in bathymetry, water quality, water clarity, impacts on engineering structures, and defence applications (Irish and White, 1998; French and Burningham, 2009; Whitehead *et al*., 2009; Kadiri *et al*., 2012). Globally, it is practically impossible to compile an accurate picture of sediment transport, though it has been estimated that 70 % of the worlds sandy beaches have shown net erosion in recent years (Bird, 1985). Despite the obvious importance of sediment transport, predictive computational models are rarely accurate to better than a factor of two, with greater uncertainty when bedforms are present, therefore field measurements continue to be required for both site specific model tuning and validation (Davies *et al*., 2002). Further, it is now widely recognised that to improve large scale sediment transport modelling, accurate parameterisations of small scale sediment processes are fundamental (Baumert *et al*., 2000; James, 2002; Ribberink *et al*., 2008; Amoudry and Souza, 2011). At present however, quantification and understanding of sediment transport processes is hampered by the difficulty in obtaining suitable measurements. At the kernel of this problem, is that suspended sediments show complex variability over multiple spatial dimensions (Hay and Bowen, 1994; Villard and Osborne, 2002; Williams *et al*., 2003), whilst most traditional measurement techniques, such as water sampling, optical backscatter sensors, and transmissometers, provide only point measurements.

Optical imaging techniques, such as Particle Image Velocimetry (PIV), provide one opportunity by which measurements of suspended sediment concentration and velocity can be obtained in two-dimensions, over a horizontal and vertical slice in the near-bed region

(Liu and Sato, 2005; Reidenbach *et al*., 2010). However, most PIV instruments are too large and intrusive for deployment in the field, and only recently have smaller autonomous systems become available (Liao *et al.*, 2009). Nevertheless, PIV can be impaired at higher suspended sediment concentrations due to increased optical attenuation and particle overlap problems (Lee *et al*., 2009), whilst at lower concentrations the addition of seeding material may be required to overcome low signal-to-noise ratios (Coupland and Pickering, 1988).

As an alternative to optical imaging, acoustic profiling techniques have received growing recognition over the last three decades, in part due to a robust theoretical basis, the development of new technology, and the non-intrusive nature of the measurements (Thorne and Hanes, 2002; Hurther *et al*., 2011). In the marine environment, most inorganic sand sized sediments have material densities and compressional sound velocities that are ~ 2.5 to 5 times greater than that of seawater, and hence suspended sands are relatively strong scatterers of underwater sound at MHz frequencies (Hay, 1991; Schaafsma and Hay, 1997; Thorne and Meral, 2008; Moate and Thorne, 2012). To exploit this principle, a number of monostatic multi-frequency Acoustic Backscatter Systems (ABS) have been developed to observe suspended sediments in the bottom 1 to 2 m above the seabed (Hess and Bedford, 1985; Vincent and Green, 1990; Hay, 1991; Schat, 1997; Thorne and Hardcastle, 1997). Since their inception, ABS have gained broad utility within sediment transport studies by underpinning a variety of observations, from sand transport fluxes in the coastal zone (Vincent *et al*., 1991), and the dependence of sediment diffusivity on grain size (Thorne *et al*., 2009), to sediment entrainment processes under irregular waves (O'Harra-Murray *et al*., 2011).

One limitation of conventional ABS is that they provide profiles in only one dimension, typically in the vertical. This design limitation arose primarily from technical constraints coupled with the desire to observe theoretical vertical variations in the suspended sediment concentration field, associated with the presence of bedforms and the bottom boundary layer

(Hess and Bedford, 1985; Lynch *et al*., 1997; Villard *et al*., 2000). To try and circumvent this limitation, a number of studies have used one-dimensional ABS measurements to probe sediment processes in two dimensions, by either mounting several transducers inline above specific bed features (Villard and Osborne, 2002), or by considering time averaged ABS data phase locked to orbital velocities and referenced to a common bed feature (Davies and Thorne, 2005; O'Harra-Murray *et al*., 2011; Hurther and Thorne, 2011). Whilst these approaches have met with some success, they are still limited in that they cannot provide synoptic two dimensional images over multiple ripple wavelengths.

In this paper, we evaluate a new, two-dimensional ABS; the Bedform And Suspended Sediment Imager (BASSI), and present results from a field deployment. The BASSI provides an essentially synoptic acoustic curtain over a two-dimensional vertical slice of the near bed water column, with centimetric resolution over intra-wave and turbulent timescales. Here, we first evaluate BASSI measurements of bedforms and suspended sediments relative to two proven commercially available acoustic backscatter instruments, deployed in a sandy intertidal zone of a macro-tidal estuary. By calculating acoustic inversions on calibrated BASSI data, we present two dimensional images, and image sequences, of suspended sandy sediments in an environment where both waves and tidal currents contribute to the near bed hydrodynamics.

2. Description of the Bedform And Suspended Sediment Imager (BASSI)

2.1. System overview

The BASSI consisted of three transducer line arrays, each of which was connected to a single electronic scheduling unit that controlled the sampling parameters. A schematic of the system is presented in Figure 1, showing only a single transducer array for clarity. Each transducer array housed 15 individual narrow beam disc transducers that functioned at fixed operating frequencies, with three different frequencies interleaved across the array; these were 2.5, 1.25, and 0.75 MHz (see Figure 1). The transducer arrays were designed to be compact, being 0.5 m long, 0.14 m wide and 0.07 m in depth, to minimise any hydrodynamic impact of the arrays on the sediment processes being measured. In the present study the three transducer arrays were connected inline, and the complete system consisted of 45 transducers spaced regularly at 3.3 cm intervals over a 1.5 m range in the horizontal.

The scheduling unit included a programming interface, to facilitate autonomous deployments. In the present study, the BASSI was programmed for hourly bursts of 55 minutes in duration, over a 1 metre vertical profile, with a vertical spatial resolution of 1 cm and a pulse repetition frequency of 32 Hz. Each recorded profile was an average over 8 successive transmissions, with the recorded profile rate being 4 Hz. The scheduling unit included additional sensors for temperature and pressure, although in the present study these sensors were only used for comparison with data obtained from higher temporal resolution instrumentation and are not presented here. When operating autonomously, the BASSI was powered by an external 15 V battery, with a total current consumption of ~ 650 mA when active and logging data, enabling deployment over multiple tidal cycles.

2.2. Transmit/receive and logger specification

For each transducer array, all functions were controlled by an internal microprocessor, including the generation of the three operating frequencies, and the digitisation of the receiver outputs by an onboard 10 bit analogue to digital (A/D) converter. The circuitry was identical for the three operating frequencies, consisting of frequency dedicated pre-amplifiers connected to a differential bandpass filter, with the output signals then input to logarithmic amplifiers. Logarithmic amplifiers were used to provide a large dynamic range, being ~ 90 dB here. Only the values of the transmitter tuning capacitors, the receiver coupling capacitors, and the bandpass filter components differed for the different operating frequencies. Receiver gain varied across the different operating frequencies, being +6 dB and -6 dB at 2.5 and 0.75 MHz respectively, relative to the 1.25 MHz signal.

When transmitting, the system energised only one group of three frequencies at once, being three adjacent transducers in a given line array, and stored the receiver output in internal memory before advancing along that array to the next group of three frequencies. Hence, 5 transmit/receive cycles were required to sample across the whole array, and this operation mode minimised cross talk and reverb across the system. Following data capture, the data were converted to 16 bit linear numbers onboard, and an average over 8 successive transmissions calculated and then written to internal USB flash drives with sufficient storage to enable the instrument to be deployed for multiple tidal cycles. When multiple transducer arrays were connected, as was the case here, then all arrays operated in parallel. Any acoustical or electrical cross talk between the individual transducer arrays when operating in parallel was minimised by having narrow, -3dB half beam widths, for the 0.75, 1.25, and 2.5 MHz transducers of 2.9°, 2.3° and 1.7° respectively, and independent transmitting and receiving electronics for each array. No cross-talk was identified in the data analysis.

The scheduling unit allowed the transmit pulse length to be specified, and this was chosen to be 20 μs as this matched the bandwidth of the logarithmic receivers. The scheduling unit also allowed an additional transmit delay between successive pulses to be specified, primarily to allow reverb to fully dissipate when working with the system in shallow bounded test tanks. In the present field study this transmit delay was set to the minimum value possible, being 0.1 ms.

3. Study site and Methods

3.1. Study site

The BASSI was deployed during spring tides between 22nd and 24th November 2011 in an intertidal area of the Dee estuary, U.K., close to the South-East tip of Hilbre island (see Figure 2). The Dee is a macro-tidal funnel shaped estuary approximately 30 km long and 8.5 km wide at the mouth. The tidal range at the mouth is 8 to 9 m on spring tides with tidal currents reaching 1.5 m/s in the nearby Hilbre channel, though in the intertidal area utilised in this study tidal currents rarely exceed 0.7 m/s. The mean freshwater river discharge into the estuary is 31 m^3/s, equating to only ~0.35 % of the tidal prism over a typical tidal cycle (Moore *et al*., 2009). Sediments in the Dee include both sand and mud sized deposits with compositional analysis suggesting that the sediments in the lower estuary are predominantly supplied from the adjacent Irish Sea (Turner *et al.*, 1994). Water depth at the deployment location was of the order ~3 m at high water on spring tides, with the instruments being submerged for typically only 4 hours per tidal cycle. In addition, the first hour of data from each tidal cycle was not used here, to prevent introducing any data contamination by flotsam from the incoming tide, or bubbles generated by waves breaking over the frame in the early stages of submergence. In the present study, the deployment location and frame orientation was specifically selected so that the BASSI array spanned a range of bedform scales found at the edge of a localised drainage channel, aligned with the dominant flood/ebb tidal flow, as shown in Figure 2.

3.2. Deployment frame and instrument suite

The BASSI was deployed on the NOC SEDbed frame; **S**ediment **E**xperiments on **D**ynamics and **bed**forms, a novel frame specifically designed to minimise the impact of the

frame and instrument casings on near bed sediment transport processes as illustrated in Figure 2c. To support the calibration, evaluation, and interpretation of the BASSI data, a range of supporting instruments were attached to the deployment frame and the relative locations of each instrument are shown in Figure 3, with the operating frequency and sampling regimes of each instrument presented in Table I. The supporting instruments included a three-dimensional acoustic ripple profiler (3D-ARP), an AQUAtec AQUAscat ABS, a Sontek Acoustic Doppler Velocimeter (ADV), a prototype Acoustic Doppler Velocity Profiler (ADVP), and a proto-type Multi-stage Static Sediment Trap (MSST). The MSST was emptied upon recovery of the instrument frame on 24/11/2011, with traps 3 to 6 containing between 5 to 15 g of sediment each, though traps 1 and 2 contained no sediment. In addition, grab samples were collected by hand at low water under and around the instrument frame, to aid in the characterisation of the local sediments. A type-C LISST was also included on the battery pack part of the deployment frame (see Figure 3), however due to optical alignment issues, and possible shielding of the sensor volume beneath the battery packs, no confidence was placed in the resulting LISST data. The present paper focuses on the evaluation and analysis of the BASSI and the following three sections detail the analysis undertaken in support of this aim.

3.3. Bedform analysis

With the BASSI's transducers being near to each other and regularly spaced, the bed echo from each recorded image provided near-synoptic profiles of the bedforms over a 1.5 horizontal transect, collocated with measurements of the suspended sediments directly above these bedforms. It was therefore considered useful to evaluate the ability of the BASSI to extract meaningful information about the measured bedforms, particularly given its relatively

coarse 1 cm vertical resolution, and 3.3 cm resolution in the horizontal (the spacing between adjacent transducers).

To extract the bed profile from the BASSI data, successive images were averaged over a 30 second period prior to bed detection. Temporal averaging was carried out to reduce noise in the detected BASSI bed location associated with the intermittent presence of suspended sediment events at the seabed. For each 30 second mean bed location, macro bed trends were removed by application of a running average, using a window size of at least one (macro) ripple wavelength, obtained from initial inspection of the data. The detrended BASSI ripple profiles were then analysed for ripple height and ripple length by application of a Fourier Transform to obtain the amplitude and frequency of the peak in the ripple spectra.

In the present study, the bedforms measured by the BASSI were evaluated relative to those measured by the 3D-ARP. The 3D-ARP is a commercially available instrument, designed specifically for obtaining acoustic profile measurements of seabed ripples in three-dimensions, and the basic operating principles have been presented previously (Marten, 2010). The 3D-ARP used here operated at 1 MHz and provided measurements of the bedforms at 0.5 cm resolution in the vertical, and 1 cm resolution in the horizontal, over a horizontal footprint 2.5 m in diameter. Here, the 3D-ARP was programmed to collect an image of the bed every 30 minutes, and for the above settings, the time taken to collect each complete bed image was approximately 13 minutes. Ripple profiles and dimensions were obtained from the 3D-ARP following essentially the same procedure as outlined above for the BASSI, with macro bedtrends being removed from the bed image before application of a Fourier Transform to obtain ripple dimensions as described above.

Hence, the BASSI obtained bedform measurements from a 1D transect every 30 seconds, whilst the 3D-ARP obtained measurements from a 2D swath every 13 minutes. Therefore, in order to compare the BASSI ripple profiles and dimensions with those obtained from the 3D-

ARP, only the section of the 3D-ARP bed image that corresponded to the location of the BASSI transect was utilised in the comparison, and the BASSI results were averaged over the same 13 minute period for which the 3D-ARP was operational.

3.4. Sediment characterisation at the study site

3.4.1. Mineralogical composition and particle size distribution

As recent studies have shown that the acoustic properties of sediments are a function of their mineralogical composition (Moate and Thorne, 2012 and 2013), the mineralogical composition of the local sediments was determined via X-ray diffraction (XRD). XRD analysis was undertaken on 5 g sub-samples of the sediment grab samples. Prior to analysis subsamples were ground in distilled water for 5 minutes and dried overnight at 60°C. The XRD analysis showed the sediments at the deployment location consisted mainly of quartz (87 to 89 % by mass), with feldspars (9 to 12 %) and calcite (1 to 2 %) also present in measurable quantities. Calcite was present in the grab samples in the form of shell fragments, and visually appeared to dominate the very coarse sand sized fraction (Wentworth, 1922). Clay minerals were detected only in trace quantities, with chlorite the most abundant clay mineral identified.

Particle size spectra were obtained for all grab and sediment trap samples using a Beckman Coulter LS-200 Laser Granulometer (CLG), in the size range 0.4 – 1900 μm. CLG samples were kept moist from initial collection in the field, and treated with a dispersing agent to break up any aggregates before being introduced into the Coulter sample port. The dispersing agent used was Calgon, being a solution of Sodium hexametaphosphate and Sodium carbonate. Duplicate size spectra were obtained from all samples and care was taken to ensure the obscuration was within instrument tolerance (8 to 12 %). As laser particle size inversion software typically assumes a spherical particle shape (Agrawal *et al*., 2007), whilst

natural sand grains are irregularly shaped, a number of samples were also sieved to provide an independent estimate of particle size spectra for comparison with those obtained using the Coulter.

Particle size distribution spectra typical of those obtained from the grab and sediment trap samples are illustrated in Figure 4. Particle size spectra in Figure 4 are expressed as relative abundance to facilitate comparison between the different particle sizing methods used. Relative abundance was calculated from the volume of each size class (or mass for sieved spectra), normalised by the maximum volume (or mass) observed in each distribution. The particle size spectra shown in Figure 4b were obtained from sediment trap 3, being the only sediment trap located beneath the BASSI and ABS to collect sufficient sediment for analysis (at 0.5 m above the bed, see Figure 3). In general, the degree of agreement between the different particle sizing methods observed in Figure 4 was encouraging, given the differences between the methods. Figure 4a shows the bed sediments were comprised of predominantly fine to medium sand, with no particles finer than medium silt observed from the sieve analysis. Figure 4b shows the suspended sediments were dominated by fine sands, with the Coulter spectra obtained from traps 4 and 5 (data not shown) being virtually identical to that obtained from trap 3. In agreement with the XRD analysis (see above), both the Coulter and sieving analysis suggested a lack of clay sized material, < 2 % by volume from the Coulter, and with only ~ 1.1 % by mass of the sample sieved from trap 3 being finer than 20 μm.

3.4.2. Modelling of the suspended sediment particle size distribution

As measurements of particle size for both seabed and suspended sediments were available here, and as the focus of the present study was to evaluate and cross-calibrate the BASSI, we elected to follow a simplistic approach to calculating the suspended sediment field by modelling a single, time averaged suspended particle size. This approach offered the

advantage of simplifying the cross-calibration procedure, by precluding any difficulties associated with possible ambiguities in an explicit acoustic inversion for both concentration and size, as discussed elsewhere (Thorne *et al*., 2011; Thorne and Hurther, 2014). Hence, the mean particle size profile was modelled following Thorne *et al*. (2002):

$$a_m = a_r \left(\frac{z}{z_r}\right)^{-l} \tag{1}$$

where a_m was the mean particle size at height z above the bed, and a_r was the mean size at the reference height, z_r = 1 cm. The parameter l was used to adjust the mean size profile so that a_m matched the mean size observed from the sediment trap (trap-3) and grab samples as end members for the profile, with the assumption that the size distribution at z_r could be approximated to equal that in the bed. Here, a value of a_r = 82.5 μm and l = 0.09 was found to reproduce the observed size profile satisfactorily. With the mean size profile determined, a log-normal size distribution was calculated for each mean size at each height above the bed, using Equation 2:

$$n(a) = \frac{1}{a\sqrt{2\pi\xi}} e^{-(log_e(a-m_0))^2/2\xi^2} \tag{2a}$$

with
$$\xi = \sqrt{log_e(\sigma_0^2 + 1)} \tag{2b}$$

and
$$m_0 = log_e\left(\frac{a_m^2}{\sqrt{a_m^2 + \sigma^2}}\right) \tag{2c}$$

and
$$\sigma_0 = \sigma / a_m \tag{2d}$$

where $n(a)$ was the probability density function (PDF) at radius a, and σ and σ_0 are the standard deviation and relative standard deviation of the distribution respectively. Here, a value of $\sigma_0 = 0.3$ was used, being the value of σ_0 observed from the particle size analysis.

3.5. Cross-calibrating the BASSI and calculation of suspended sediment concentrations

3.5.1. Acoustic theory and instrument calibration

For a suspension of sediments, with mean size a_m, and at concentrations low enough for multiple scattering to be ignored, the root-mean-square (RMS) backscattered voltage recorded from a piston transducer, V_{RMS}, can be written as (Hay, 1991; Thorne and Hanes, 2002):

$$V_{RMS}(r) = \frac{K_t f_N \sqrt{M(r)}}{\psi r \sqrt{a_m(r)}} e^{-2\alpha r} \tag{3a}$$

with

$$f_N = \frac{f_0}{\sqrt{\rho}} \tag{3b}$$

and

$$\alpha = \alpha_S + \alpha_W \tag{3c}$$

and

$$\alpha_S(r) = \frac{3}{4r} \int_0^r \frac{M(r)\chi_N}{a_m(r)} dr \tag{3d}$$

with

$$\chi_N = \frac{\chi_0}{\rho} \tag{3e}$$

where $M(r)$ is the suspended sediment concentration at range r, ψ is dimensionless and accounts for the transducer near field correction, f_0 is the ensemble backscattering form function, ρ is the grain density of the sediments in suspension, α_S is attenuation due to sediment scattering, a_W is the water absorption (taken from Francois and Garrison, 1982), and

χ_0 is the ensemble normalised total scattering cross section. In order to extract suspended sediment concentrations from ABS data, estimates of the electronic calibration coefficients, K_t, are required. These calibrations incorporate the receiver sensitivity, the electronic gain, and the transducer beam pattern characteristics (Thorne and Hanes, 2002).

For the AQUAscat, calibrations were determined for each transducer following the procedure detailed in Betteridge *et al*. (2008). However, the physical dimensions of the BASSI precluded calibration in this way, since the arrays were too large to fit into the relatively narrow sediment tower calibration tank (see Betteridge *et al*., 2008, for a full description of this facility and the calibration procedure). Therefore, the approach taken in the present study was to use the calibrated AQUAscat to cross-calibrate the BASSI in the field. This was achieved by using the modelled suspended sediment size profile to calculate a nominal, time averaged description of the suspended sediment concentration field from the laboratory calibrated AQUAscat. The procedure followed to calculate suspended sediment concentrations is described in the next section. Hence, K_t coefficients were obtained for the BASSI by rearranging Equation 3, thus:

$$K_t = \frac{V_{RMS}\psi r\sqrt{a_m}}{f_N\sqrt{\langle M\rangle}}e^{2\alpha r} \tag{4}$$

where the <> brackets denote a temporal average. Thus, the BASSI data was temporally averaged over the same time intervals as the AQUAscat data, and the appropriate <*M*> from the AQUAscat used to obtained profiles of K_t for each BASSI transducer using Equation 4. As the BASSI employed a constant gain for each transducer, the resulting profiles of K_t could reasonably be expected to be invariant with range, thus providing one test by which the validity and robustness of the above procedure could be evaluated.

3.5.2. Calculation of time averaged suspended sediment concentrations

For a range gated ABS profile, Equation 3 can be solved for M at range r_i by rearranging into the form:

$$M(r_i) = v_1(r_i)e^{v_2(r_i)M(r_i)} \tag{5a}$$

with $$v_1(r_i) = \frac{(V_{RMS}(r_i)\psi r_i)^2 a_m(r_i)}{K_t f_N} e^{4\alpha_W r_i} e^{3\Delta r \sum_{r=r_1}^{r=r_{i-1}} \frac{M(r)\chi_N}{a_m(r)}} \tag{5b}$$

and $$v_2(r_i) = \frac{3\chi_N \Delta r}{a_m(r_i)} \tag{5c}$$

where all terms are as previously defined and Δr is the range gated bin. Thus, to calculate the parameters v_1 and v_2 requires knowledge of the ensemble scattering properties of the suspended sediments, χ_0 and f_0, and hence a_m and the size distribution which were modelled here using Equations 1 and 2. The ensemble scattering properties are obtained by integrating the intrinsic scattering properties, χ and f, over $n(a)$ provided by Equation 2 (Sheng and Hay, 1988; Thorne and Campbell, 1992; Moate and Thorne, 2009). For the intrinsic scattering properties, we used the generic scattering formulations recently presented in Moate and Thorne (2012), which provide a heuristic description of these properties, normalised by grain density. Hence, with all the input parameters defined, Equation 5 is in a form that can be solved iteratively using the Newton-Raphson formulation:

$$M(r_i)_j = M(r_i)_{j-1} - \frac{M(r_i)_{j-1} - v_1(r_i)e^{v_2(r_i)M(r_i)_{j-1}}}{1 - v_1(r_i)v_2(r_i)e^{v_2(r_i)M(r_i)_{j-1}}} \tag{6}$$

where j defines the iteration level and Equation 6 is iterated until a convergence criterion is achieved. For the present dataset, convergence typically occurred after no more than six iterations, and following this procedure, $M(r_i)$ was calculated step-wise along the ABS profile, from i=1 to i=b-1, where b denotes the bin at which the bed echo was observed. To obtain time averaged suspended sediment concentrations using Equations 5 and 6, V_{RMS} is simply calculated over the desired time window. For the inter-calibrations in the present study, we calculated V_{RMS} over 5 minute periods for each burst, to remove fluctuations associated with processes operating at turbulent and wave period timescales.

4. Results

4.1. Evaluation of the BASSI measurements

4.1.1. Bedform dimensions

Measurements from the 3D-ARP showed small scale ripples dominated the bedforms throughout the deployment with ripple amplitude rarely exceeding 2 cm. This was in agreement with bedform observations made by eye during low water inspections, as shown in Figure 2c. Figure 5 presents a 3D ripple image typical of those observed by the 3D-ARP, and compares ripple measurements obtained from both the 3D-ARP and BASSI. A mixture of 2D and 3D ripple types can be seen in Figure 5a, with the maximum departure from mean bed level being ± 0.06 m. The two features at ~ 0.5 m along frame distance in Figure 5a were caused by scattering from the instrument frame legs and their associated near-bed stabilising weights (see Figure 2c). Figure 5a illustrates the location of the BASSI bed profile within the 3D-ARP footprint, shown by the solid white line, and a comparison between the ripple profiles observed by the two instruments is presented in Figure 5b, for the same burst as shown in Figure 5a. Figure 5b shows the BASSI and 3D-ARP observed essentially the same time-averaged bed profile with the degree of agreement observed in Figure 5b being typical of the dataset collected in the present study. The shaded area in Figure 5b shows ± two standard errors about the time-averaged BASSI bed profile and illustrates the relative stability of the bedforms during the time taken to collect the 3D-ARP bed image, at this stage of the tidal cycle.

Measurements of the nominal ripple height and wavelength obtained from each time-averaged BASSI bed profile were also evaluated relative to those obtained by the 3D-ARP, across all four tidal cycles, shown in Figure 5c. Figure 5c shows BASSI ripple dimensions compared well with those observed by the 3D-ARP, with most of the field data scattered

within ± 20 % of the 1:1 line in Figure 5c. Whilst the 3D-ARP observed a number of ripple heights between 0.6 and 0.9 cm during the deployment, the minimum ripple height observed by the BASSI was ~ 1 cm (see Figure 5c). This lower limit to the BASSI ripple heights could reasonably be expected, given the vertical resolution of the BASSI in the present study was 1 cm.

4.1.2. Backscatter measurements above the bed

As an initial check of the veracity of the BASSI measurements the raw backscattered voltages were compared with those recorded by the AQUAscat, as a function of time and height above the bed. For the deployment reported here, only the 2.5 MHz operating frequency was common to both instruments (see Table I), and hence direct comparisons were only possible for BASSI transducers operating at this frequency. As the two instruments were not co-located, the root-mean-square backscattered voltage, V_{RMS}, calculated over 5 minute periods were compared, to remove small scale variability associated with processes operating over turbulent and wave period timescales. In addition, because the two instruments employed differing transmit and receive systems, for the purpose of comparison, V_{RMS} was normalised by the maximum observed V_{RMS} in the period of interest. Hence, a comparison of normalised V_{RMS} obtained from both instruments is presented in Figure 6 for one of the four tidal cycles sampled. Figure 6 shows measurements from three BASSI transducers regularly spaced across the 1.5 m length of the BASSI array, at three different vertical ranges. Figure 6 generally shows close agreement between the two instruments, along the length of the BASSI array, throughout the tidal cycle, and for all three heights above the bed. The closest agreement between the two instruments was observed for the measurements obtained closest to the bed, Figure 6a. This may indicate that the BASSI had a slightly higher noise floor than

the AQUAscat, since suspended sediment concentrations were typically greatest in the near-bed region, thereby giving rise to a greater signal to noise ratio in this region.

4.2. Cross-calibration of the BASSI

4.2.1. The nominal, time averaged suspended sediment concentration field

Figure 7 presents an illustrative time series of suspended sediment concentration obtained from the AQUAscat, $<M>$, with V_{RMS} again calculated over 5 minute intervals and the angular brackets <> denoting a time-average estimate. The data presented in Figure 7 were obtained from the same tidal cycle for which V_{RMS} was presented in Figure 6. In Figure 7a, $<M>$ was obtained by inverting the multi-frequency AQUAscat data using Equations 5 and 6, with the suspended size distribution provided by Equations 1 and 2, following the procedure detailed in Section 3.5.2. The three vertical white bands in Figure 7a correspond to the inactive periods at the end of each hourly burst, whilst the regions below approximately 0.5 m range correspond to the detected seabed location. To aid interpretation of $<M>$, the velocities and pressure recorded by the ADV, time-averaged over the same 5 minute intervals, are presented in Figure 7b and 7c. Figure 7 shows a clear tidal variation in $<M>$ was present, with a waxing and waning pattern in the suspended sediment concentration either side of high water slack, with increases in $<M>$ occurring at the same times as peaks in cross-frame velocity. In addition, Figure 7a shows a clear vertical gradient in $<M>$ with height above the bed, with the range of $<M>$ observed being ~ 0 to 0.4 g/l, consistent with those observed in previous acoustic studies of near-bed suspended sediment concentrations (Vincent and Green, 1990; Hay and Sheng, 1992; Thorne and Hardcastle, 1997; Hurther *et al*., 2011). The suspended sediment field presented in Figure 7 was typical of that observed for the other tidal cycles sampled in the present study, both in terms of the temporal variation

across the tidal cycles, and the magnitude of the suspended sediment concentrations obtained from the AQUAscat.

4.2.2. BASSI calibration profiles and mean coefficients

The nominal frequency-averaged suspended sediment concentrations from the AQUAscat described above were thus used to calculate profiles of K_t for the BASSI using Equation 4. Figure 8 presents BASSI K_t profiles obtained in this way from the central transducer array, grouped by operating frequency. The different symbols in Figure 8 show an average K_t profile for each of the transducers present in the central array (hence, 5 for each frequency). These average K_t profiles were calculated from BASSI data collected from the first hour of the ebb tides, with data taken from each of the 4 tidal cycles for which the BASSI was deployed. This stage of the tidal cycle was chosen as it was observed to produce a high signal to noise ratio with maximum suspended sediment concentrations, as can be seen for example between 10:00 and 11:00 in Figure 7a. Figure 8 shows the resulting K_t profiles obtained from the BASSI were nominally invariant with both range and between individual transducers of the same operating frequency, with differences between transducers of the same frequency being of the same order as the uncertainty in laboratory measurements of K_t reported elsewhere; ~ 5 % (Moate and Thorne, 2013). Thus, as no significant differences were observed in K_t between transducers of the same operating frequency, an overall mean K_t was calculated for each operating frequency for each transducer array. The solid lines in Figure 8 show the overall mean K_t coefficient for each operating frequency in the central array and these values are annotated in each plot along with their associated standard deviations.

4.3. Inversion results from the BASSI

4.3.1. Inter-comparison of time-averaged sediment concentrations obtained from BASSI and AQUAscat ABS

With K_t determined for each transducer in the BASSI array, estimates of suspended sediment concentration were obtained from the BASSI following the implicit inversion methodology detailed in Section 3.5.2. As in Section 4.2.1, inversion estimates were again obtained from V_{RMS} calculated over 5 minute periods to remove variability over turbulent and wave period timescales, providing time averaged suspended sediment concentrations. Figure 9 presents a comparison of $<M>$ obtained from the BASSI and AQUAscat ABS, as an appraisal of the BASSI performance over the range of near-bed suspended concentrations encountered in the Dee. Whilst the BASSI calibration constants, K_t, were obtained from only part of the tidal cycle, the aim of the comparison shown in Figure 9 was to evaluate the veracity of the BASSI inversions across the whole tidal cycle and therefore a much greater variation in $<M>$ than for the calibration period. The BASSI inversion estimates shown in Figure 9 were obtained from the middle three transducers of the central array, being in-line with the AQUAscat in the along frame direction, and are compared to the frequency averaged inversion estimates from the AQUAscat. In Figure 9a, comparisons are shown at a height of 10 cm above the detected bed location, for each of the 5 minute mean profiles obtained from each burst from each of the four tidal cycles. Figure 9a shows close agreement between the BASSI and AQUAscat suspended sediment concentration estimates, with concentrations ranging over two orders of magnitude. The dashed lines in Figure 9a show ± 40 %, with 84 %

of the BASSI concentrations being within 40 % of those obtained from the AQUAscat, and 95 % being within a factor of two. There is some evidence in Figure 9a that <*M*> obtained from the 0.75 MHz transducer compared less favourably with the AQUAscat estimates than concentration obtained from the other BASSI operating frequencies.

Figure 9b presents a comparison of profiles of time and frequency averaged suspended sediment concentration obtained from both the BASSI and AQUAscat, at four times across the tidal cycle. For the BASSI, inversion estimates obtained from the central 1.25 and 2.5 MHz transducers were averaged, with those for the AQUAscat obtained from the 1 and 2.5 MHz transducers. Figure 9b shows encouraging agreement throughout the length of the profiles, across the tidal cycle, and for concentrations ranging over two orders of magnitude. As in Figure 7, the magnitude of the BASSI suspended sediment concentrations shown in Figure 9 were consistent with those typically encountered in shallow marine waters (Vincent and Green, 1990; Hurther *et al*., 2011).

4.3.2. Suspended sediment concentrations in 2D-HV

As an operational appraisal of the synoptic spatial imaging of suspended sediment variability observable with the BASSI in 2D-HV, Figure 10 presents a time sequence of images of suspended sediment concentration obtained over the near-bed region at the study site in the Dee. The images presented in Figure 10 were obtained over a 3.5 s period at the times annotated in each panel, near slack water on the 22/11/2012. The suspended sediment concentrations presented in Figure 10 were obtained by inverting the recorded backscatter, being an average over 8 succesive pings (see Section 2.1), following the same inversion methodology as described above (see Section 3.5.2). The resulting suspended sediment concentrations are presented in Figure 10 logarithically transformed to base 10, to enable variations over multiple magnitudes to be clearly discerned. For ease of reference, on the

colour scale shown in Figure 10, -3 is equivilant to 0.001 g/l and -0.5 is equivilant to 0.3 g/l; being the same range as was observed for inversion results presented in Figure 9a.

The ADV deployed on SEDbed (see Figure 3) showed near bed flow was dominated by wave orbital velocities around slack water at the study site, and hence the across frame velocity component is annotated in Figure 10 for the same times at which the BASSI images were obtained. It should be noted that the ADV sampling volume was located approximately 40 cm above the bed and therefore the magnitude and direction of the velocity vectors illustrated in Figure 10 are only presented as an indication of the relative strength and direction of flow in each panel.

There are four key points that can be observed in Figure 10. The first is that suspended sediment concentrations nominally display the usual variation observed in the vertical, with concentrations typically increasing towards the bed. The second is that this is not always the case, with occasional pockets of relatively high suspended sediment concentration located approximately mid-water, for example at 0.07 m horizonatal range in Figure 10b. Thirdly there are clear variations in suspended sediment concentration in the horizontal near the bed, with a waxing and waning of concentrations that appears to have a horizontal periodicity similar to the wavelength of the bedforms, this can clearly be seen in Figure 10c. Finally, by studying the image sequence shown in Figure 10, it can be seen that the horizontal variations in suspended sediment concentration do not occur at static locations, but rather there appear to be event packets of suspended sediments that are being advected, or entrained, with the flow. To illustrate this, three packets have been labelled A, B, and C in Figure 10. In Figure 10a to 10c, these packets are successively advected to the right, reduce or settle out in Figure 10d, with packet B being advected back to the left in Figure 10e and 10f.

5. Discussion

Nearbed sediment entrainment, transport and deposition over bedforms are spatially and temporally variable with dynamic interactions between the hydrodynamics, the bedforms and the sediment transport. Contemporary measurement systems usually provide 1D-V observations of sediment processes at one location above the bed. To extend beyond 1D-V, the BASSI acoustic array has been developed to provide measurement of suspended sediments simultaneously over a transect of the bed. The technology builds upon the 1D-V ABS systems which have been under development over the past two to three decades. To calibrate and assess the BASSI, the array was deployed with a number of supporting instruments on the SEDbed frame in a macro-tidal estuary. The selected deployment location had a sandy bed and the local hydrodynamics were sufficient to entrain the bed sediments into the water column, providing an ideal testing ground for this new technology.

Significant effort was made to deploy the instruments on a frame that would minimise frame effects on the bed, such as those described by Bolaños *et al*. (2011). To this end, over a series of pilot studies, the SEDbed frame was developed for the present study. Figure 2c illustrates the low impact of SEDbed on the local seabed and this image is consistent with a series of observations made by the authors, carried out at low water periods during previous deployments and the deployment reported here. Additionally, and also in the interests of ensuring data quality; substantial care was taken when selecting the locations and sampling settings of the various instruments attached to the frame, to avoid instrument interference. Where operating frequencies were common between two instruments, these were set at opposite ends of the frame, for eaxmple the AQUscat ABS and 3D-ARP (Table I; Figure 3). No evidence of instrument interference was apparent in the instrument data, and we believe these effects have been minimised in the present study. Thus, SEDbed and its main payload

of acoustic instruments were successful in providing a non-intrusive platform in the Dee, enabling acoustic remote sensed measurements of the flow, the suspended sediments, and the bedforms.

The close agreement between the BASSI and 3D-ARP measurements of bedforms shown in Figure 5 is encouraging. Given the repeated triplet of frequencies in use across the BASSI array, Figure 5 suggests the accuracy of the bed location obtained from the BASSI was independent of operating frequency. Figure 5 shows some differences in the detected bed location were observed between the BASSI and 3D-ARP. These differences are relatively minor however and could reasoably be expected to occur given the differences in sampling time, and the differences in the relative angles between the sensors and bedforms for the two instruments. As commented in Section 4.3.1, Figure 5c shows that the smallest ripple height resolved by the BASSI was ~ 1 cm, being the vertical resolution of the BASSI profiles. Whilst not observed in the present study, this suggests that there will also likely be a lower limit to the minimum ripple wavelength resolvable by the BASSI, likely to be of the order of 5 cm, being approximately twice the horizontal spacing of the BASSI transducers along the array. Whilst acoustic transects of rippled bedforms have been studied previously (Thorne *et al.*, 2003; Soulsby *et al*., 2012; Miles and Thorpe, 2015), the quality unique to BASSI is the ability to obtain measurements of the suspended sediments directly referenced to simultaneously measured bedforms over a horizontal transect. The spatial transitions in suspended sediment concentration observed in Figure 10 are evocative of observations of sediment entrainment observed elsewhere (O'Hara Murray *et al*., 2011; Hurther and Thorne, 2011).

As far as the authors are aware the BASSI array uniquely generates high temporal-spatial 2D-HV images of boundary layer sediment processes for the study of sediment transport dynamics. The only previous two-dimensional acoustic studies of suspended sediments that

the authors are aware of are those presented by Simmons *et al*. (2010) and Traykovski *et al*. (2015). Simmons *et al*. (2010) used a Multi-Beam Echo Sounder (MBES) attached to a nominally stationary boat, with measurements obtained across a two-dimensional arc predominantly in the upper water column at the confluence of two river systems. In contrast, Traykovski *et al*. (2015) reported on the deployment of a horizontal array of five downward looking single beam pulse-coherent Doppler profilers used to measure the horizontal wavelength of instabilities in a lutocline. The encouraging performance of these instruments, and the BASSI presented here, opens up novel opportunities for sediment transport studies; providing new tools for the two dimensional acoustical imaging of sediment transport processes.

Finally, the aim of the present work was to develop a new, high spatial-temporal resolution, non-intrusive, acoustic array for obtaining 2D-HV measurements of bedforms and suspended sediments over a transect. The results presented here from a field study show that the BASSI is capable of obtaining such measurements. Future studies with the BASSI will investigate its ability to measure suspended particle size in 2D-HV using its multi-frequency capability, quantify ripple migration rates, utilise cross correlation and image tracking techniques to extract flow velocity information, and to delve deeper into the dynamic interrelationships between the flow, the bedforms and the sediment transport by utilising the flexibility of different array configurations.

Acknowledgements

This work was jointly funded by the UK Natural Environment Research Council as part of its small scale sediment process studies, and by the European HydralabIV-WISE programme (European Commission Contract 261520). The authors would like to thank members of the UK National Oceanography Centre for their hard work during the construction of the frame and sediment traps, as well as during the deployment and recovery of SEDbed (Terry Doyle, Chris Balfour, Daniel McLaughlin, Ray Edun, David Jones, and Emlyn Jones), and in particular Dr. Paul Bell for contributions in both the field deployments and analysis of the 3D-ARP data. The authors would also like to thank Marine Electronics Ltd for their assistance in the design, development and manufacturing of the BASSI, and Dr. James Utley, University of Liverpool, UK, for the mineralogical composition analysis of the sediment samples.

References

Agrawal, Y.C., McCave, I.N., and Riley, J.B., 2007. Laser diffraction size analysis. In: Syvitski, J.P.M. (ed.) Principle, methods, and application of particle size analysis, *Cambridge University Press*, Cambridge, 368 pp.

Amoudry, L.O. And Souza, A.J., 2011. Deterministic Coastal Morphological and Sediment Transport Modeling: A Review and Discussion. *Reviews of Geophysics*, 49, RG2002.

Baumert, H., Chapalain, G., Smaoui, H., McManus, J.P., Yagi, H., Regener, M., Sundermann, J., and Szilagy, B., 2000. Modelling and numerical simulation of turbulence, waves and suspended sediments for pre-operational use in coastal seas. *Coastal Engineering*, 41, 63-93.

Betteridge, K.F.E., Thorne, P.D. and Cooke, R.D., 2008. Calibrating multi-frequency acoustic backscatter systems for studying near-bed suspended sediment transport processes. *Cont. Shelf Res.*, 28, 227-235.

Bird, E.C.F., 1985. Coastline changes: A global review, John Wiley & Sons Ltd, 219 pp.

Bolaños, R., Amoudry, L.O., and Doyle, K., 2011. Effects of Instrumented Bottom Tripods on Process Measurements. *Journal of Atmospheric and Oceanic Technology*, 28, 827-837.

Coupland, J.M. and Pickering, C.J.D., 1988. Particle Image Velocimetry: Estimation of Measurement Confidence at Low Seeding Densities. *Optics and Lasers in Engineering*, 9, 201-201.

Davies, A.G., van Rijn, L.C., Damgaard, J.S., van de Graaff, J., and Ribberink, J.S., 2002. Intercomparison of research and practical sand transport models, *Coast. Eng.*, 46, 1-23.

Davies, A.G. and Thorne, P.D., 2005. Modeling and measurement of sediment transport by waves in the vortex ripple regime. *Journal of Geophysical Research-Oceans*, 110, C05017.

Francois, R.E., and Garrison, G.R., 1982. Sound absorption based on ocean measurements. Part I: Pure water and magnesium sulphate contributions. *Journal of the Acoustical Society of America*, 72 (3), 896-907.

French, J.R. and Burningham, H., 2009. Coastal geomorphology: trends and challenges, *Progress in Physical Geography*, 33 (1), 117-129.

Hay, A.E., 1991. Sound scattering from a particle laden, turbulent jet. *J. Acoust. Soc. Am.*, 90 (4), 2055-2074.

Hay, A.E. and Sheng, J., 1992. Vertical profiles of suspended sand concentration and size from multifrequency acoustic backscatter. *Journal of Geophysical Research*, 97 (C10), 15661-15677.

Hay, A.E. and Bowen, A.J., 1994. Coherence Scales of Wave-Induced Suspended Sand Concentration Fluctuations. *Journal of Geophysical Research-Oceans*, 99, 12749-12765.

Hess, F.R. and Bedford, K.W., 1985. Acoustic Backscatter System (ABSS): the instrument and some preliminary results. *Mar. Geol.*, 66, 357-379.

Hurther, D., and Thorne, P.D., 2011. Suspension and near-bed load sediment transport processes above a migrating, sand-rippled bed under shoaling waves. *Journal of Geophysical Research*, 116, C07001.

Hurther, D., Thorne, P.D., Bricault, M., Lemmin, U., and Barnoud, J.M., 2011. A multi-frequency Acoustic Concentration and Velocity Profiler (ACVP) for boundary layer measurements of fine-scale flow and sediment transport processes. *Coastal Engineering*, 58 (7), 594-605.

Irish, J.L. and White, T.E., 1998. Coastal engineering applications of high-resolution lidar bathymetry. *Coast. Eng.*, 35, 47-71.

James, I.D., 2002. Modelling pollution dispersion, the ecosystem and water quality in coastal waters: a review. *Environmental Modelling and Software*, 17 (4), 363-385.

Kadiri, M., Ahmadian, R., Bockelmann-Evans, B., Rauen, W., and Falconer, R., 2012. A review of the potential water quality impacts of tidal renewable energy systems. *Renewable and Sustainable Energy Reviews*, 16, 329-341.

Lee, C., Wu, C.H., and Hoopes, J.A., 2009. Simultaneous particle size and concentration measurements using a back-lighted particle imaging system. *Flow Measurement and Instrumentation*, 20 (4-5), 189-199.

Liao, Q., Bootsma, H.A., Xiao, J., Val Klump, J., Hume, A., Long, M.H., and Berg, P., 2009. Development of an in situ underwater particle image velocimetry (UWPIV) system. *Limnol. Oceanogr.: Methods*, 7, 169:184.

Liu, H.J. and Sato, S., 2005. Laboratory study on sheetflow sediment movement in the oscillatory turbulent boundary layer based on image analysis. *Coastal Engineering Journal*, 47 (1), 21-40.

Lynch, J.F., Irish, J.D., Gross, T.F., Wiberg, P.L., Newhall, A.E., Traykovski, P.A. and Warren, J.D., 1997. Acoustic measurements of the spatial and temporal structure of the near-bottom boundary layer in the 1990-1991 STRESS experiment, *Cont. Shelf Res.*, 17 (10), 1271-1295.

Marten, K.V., 2010. Field Observation and Modelling of Near-shore Sediment Transport Processes. Ph.D. Thesis. School of Ocean Sciences, *Bangor University*, UK.

Miles, J. and Thorpe, A., 2015. Bedform contributions to cross-shore sediment transport on a dissipative beach. *Coastal Engineering*, 98, 65-77.

Moate, B.D., and Thorne, P.D., 2009. Measurements and inversion of acoustic scattering from suspensions having broad size distributions. *J. Acoust. Soc. Am.*, 126 (6), 2905-2917.

Moate, B.D., and Thorne, P.D., 2012. Interpreting acoustic backscatter from suspended sediments of different and mixed mineralogical composition. *Cont. Shelf Res.*, 46, 67-82.

Moate, B.D., and Thorne, P.D., 2013. Scattering from suspended sediments having different and mixed mineralogical compositions: Comparison of laboratory measurements and theoretical predictions. *J. Acoust. Soc. Am.*, 133 (3), 1320-1334.

Moore, R.D., Wolf, J., Souza, A.J., and Flint, S.S., 2009. Morphological evolution of the Dee Estuary, Eastern Irish Sea, UK: A tidal asymmetry approach. *Geomorphology*, 103 (4), 588-596.

O'Harra Murray, R.B., Thorne, P.D., and Hodgson, D.M., 2011. Intrawave observations of sediment entrainment processes above sand ripples under irregular waves, *J. Geophys. Res*., 116, C01001.

Reidenbach, M.A., Limm, M., Hondzo, M., and Stacey, M.T., 2010. Effects of bed roughness on boundary layer mixing and mass flux across the sediment-water interface. *Water Resourc. Res.*, 46, W07530, doi:10.1029/2009WR008248.

Ribberink, J.S., van Der Werf, J.J., O'Donoghue, T., and Hassan, W.N.M, 2008. Sand motion induced by oscillatory flows: Sheet flow and vortex ripples. *Journal of Turbulence*, 9 (20), 1-32.

Schaafsma, A.S. and Hay, A.E., 1997. Attenuation in suspensions of irregularly shaped sediment particles: A two-parameter equivalent spherical scatterer model. *J. Acoust. Soc. Am.*, 102 (3), 1485-1502.

Schat, J., 1997. Multifrequency acoustic measurement of concentration and grain size of suspended sand in water. *J. Acoust. Soc. Am.*, 101 (1), 209-217.

Sheng, J. and Hay, A.E., 1988. An examination of the spherical scatterer approximation in aqueous suspensions of sand. *J. Acoust. Soc. Am.*, 83 (2), 598-610.

Simmons, S.M., Parsons, D.R., Best, J.L., Orfeo, O., Lane, S.N., Kostaschuk, R., Hardy, R.J., West, G., Malzone, C., Marcus, J., and Pocwiardowski, P., 2010. Monitoring Suspended Sediment Dynamics Using MBES. *Journal of Hydraulic Engineering*, 136 (1), 45-49.

Soulsby, R.L., Whitehouse, R.J.S., and Marten, K.V., 2012. Prediction of time-evolving sand ripples in shelf seas. *Cont. Shelf. Res.*, 38, 47-62.

Traykovski, P., Trowbridge, J., and Kineke, G., 2015. Mechanisms of surface wave energy dissipation over a high-concentration sediment suspension, *J. Geophys. Res. Oceans*, 120, 1638–1681, doi:10.1002/2014JC010245.

Thorne, P.D. and Campbell, S.C., 1992. Backscattering by a suspension of spheres. *J. Acoust. Soc. Am.*, 92 (2), 978-986.

Thorne, P.D. and Hardcastle, P.J., 1997. Acoustic measurements of suspended sediments in turbulent currents and comparison with in-situ samples. *J. Acoust. Soc. Am.*, 101 (5), 2603-2614.

Thorne, P.D. and Hanes, D.M., 2002. A review of acoustic measurement of small-scale sediment processes. *Cont. Shelf Res.*, 22, 603-632.

Thorne, P.D., Williams, J.J., and Davies, A.G., 2002. Suspended sediments under waves measured in a large scale flume facility. *J. Geophys. Res.* 107(C8), 4.1–4.16.

Thorne, P.D., Davies, A.G., and Williams, J.J., 2003. Measurements of near-bed intra-wave sediment entrainment above vortex ripples. *Geophys. Res. Lett.*, 30(20), 2028, doi:10.1029/2003GL018427.

Thorne, P.D. and Meral, R., 2008. Formulations for the scattering properties of suspended sandy sediments for use in the application of acoustics to sediment transport processes. *Cont. Shelf Res.*, 28, 309-317.

Thorne, P.D., Davies, A.G., and Bell, P.S., 2009. Observations and analysis of sediment diffusivity profiles over sandy rippled beds under waves, J. Geophys. Res., 114, C02023.

Thorne, P.D., Hurther, D., and Moate, B.D., 2011. Acoustic inversions for measuring boundary layer suspended sediment processes. *J. Acoust. Soc. Am.*, 130 (3), 1188-1200.

Thorne, P.D., and Hurther, D., 2014. An overview on the use of backscattered sound for measuring suspended particle size and concentration profiles in non-cohesive inorganic sediment transport studies. *Cont. Shelf. Res.*, 73, 97-118.

Turner, A., Millward, G.E., and Tyler, A.O., 1994. The Distribution and Chemical Composition of Particles in a Macrotidal Estuary. *Estuar. Coast. Shelf S.*, 38, 1-17.

Villard, P.V., Osbourne, P.D., and Vincent, C.E., 2000. Influence of wave groups on SSC patterns over vortex ripples. *Cont. Shelf Res.*, 20 (17), 2391-2410.

Villard, P.V. and Osborne, P.D., 2002. Visualization of wave-induced suspension patterns over two-dimensional bedforms. *Sedimentology*, 49 (2), 363-378.

Vincent, C.E., and Green, M.O., 1990. Field Measurements of the Suspended Sand Concentration Profiles and Fluxes and of the Resuspension Coefficient γ_0 Over a Rippled Bed. *Journal of Geophysical Research*, 95 (C7) 11591-11601.

Vincent, C.E., Hanes, D.M. and Bowen, A.J., 1991. Acoustic measurements of suspended sand on the shoreface and the control of concentration by bed roughness. *Mar. Geo.*, 96, 1-18.

Wentworth, C.K., 1922. A scale of grade and class terms for clastic sediments. *Journal of Geology*, 30, 377-392.

Whitehead, P.G., Wilby, R.L., Battarbee, R.W., Kernan, M., and Wade, A.J., 2009. A review of the potential impacts of climate change on surface water quality. *Hydrological Sciences Journal*, 54 (1), 101-123.

Williams, J.J., Bell, P.S., Thorne, P.D. and Humphrey, J.D., 2000. Field measurements of flow and sediment transport over complex bed morphology.

Williams, J.J., Bell, P.S., and Thorne, P.D., 2003. Field measurements of flow fields and sediment transport above mobile bed forms. *Journal of Geophysical Research-Oceans*, 108, 3109.

Tables

TABLE I – Instrument sampling parameters and operating frequencies.

Instrument	**Burst Interval (minutes)**	**Burst Duration (minutes)**	**Sampling Frequency (Hz)**	**Operating Frequency (MHz)**
BASSI	60	55	4	0.75, 1.25, 2.5
ABS	60	55	4	0.5, 1.0, 2.5
3D-ARP	30	13	-	1.0
ADV	30	27	16	5.0

Figure captions

Figure 1 – Schematic of the Bedform And Suspended Sediment Imager, showing one transducer array connected to the electronic scheduling unit, mounted above the seabed. The different coloured beams represent the different operating frequencies of 2.5 MHz (red), 1.25 MHz (green) and 0.75 MHz (blue).

Figure 2 – The study site in the Dee estuary (a), and its location relative to the adjacent Irish Sea (b), as indicated by the shaded box. A photo of the SEDbed instrument frame at low water is shown in (c), looking Northwest towards the Irish Sea. The photo in (c) was taken after two tidal cycles, and illustrates the low impact of the frame on the bed underneath the instrument sensors.

Figure 3 – Schematic of the SEDbed instrument frame, showing the relative location of the Bedform And Suspended Sediment Imager (BASSI), AQUAscat Acoustic Backscatter System (ABS), Acoustic Doppler Velocimeter (ADV), Acoustic Doppler Velocity Profiler (ADVP), three dimensional Acoustic Ripple Profiler (3D-ARP), LISST, and Multi-Stage Sediment Trap (MSST).

Figure 4 – Particle size distribution spectra obtained from (a) a seabed grab sample, and (b) MSST sediment trap 3 (see Figure 3a), collected on 24/11/2011. The median particle size, d_{50}, obtained from each method is also shown in each plot.

Figure 5 – Ripple measurements obtained from the 3D-ARP and BASSI. A ripple image typical of those observed by the 3D-ARP is shown in (a), along with the location of the

BASSI transect (white solid line). A comparison of the ripple profiles observed by the 3D-ARP and BASSI are shown in (b) for the same record as shown in (a). The shaded envelope in (b) depicts ± two standard errors about the temporal mean BASSI ripple profile. A comparison of the ripple dimensions observed by both instruments is shown in (c), with both ripple height (×10) and ripple length presented, and the theoretical 1:1 line also shown (—). The dashed lines (---) shown in (c) illustrate ± 20 % about the 1:1 line.

Figure 6 – Normalised V_{RMS} measurements obtained from the AQUAscat and BASSI on 23/11/2011. Measurements are shown at three vertical ranges, being (a) 45 cm, (b) 30 cm, and (c) 10 cm from the AQUAscat transducer. For the tidal cycle shown, high water slack occurred at ~ 08:40. All data shown were obtained at the operating frequency common to both instruments, 2.5 MHz, with data presented from three BASSI transducers located across the 1.5 m array. The cross frame distance (CFD) , relative to the centre of the BASSI array, is shown for each sensor.

Figure 7 – Time-averaged suspended sediment concentrations, $\langle M \rangle$ (a), ADV velocities (b), and ADV pressure (c), on the morning of 23/11/2011. The sediment concentrations shown in (a) can be seen to be least around high water slack, with increases in $\langle M \rangle$ coinciding with peaks in cross frame velocity seen in (b).

Figure 8 – Profiles of BASSI calibration coefficients, K_t, obtained from the central array. Profiles are shown from each transducer in the array, grouped by operating frequency, with each profile shown being the average of a number of profiles obtained across the four tidal cycles sampled. The overall mean K_t for each operating frequency is also shown (—) and annotated, along with the associated standard deviation.

Figure 9 – Comparison of inversion estimates of the time-averaged suspended sediment concentrations obtained from the BASSI at each frequency, with the time and frequency averaged concentrations obtained from the AQUAscat. In (a), comparisons are shown at a height of 10 cm above the bed for each of the 5 minute mean profiles obtained from each burst from each of the four tidal cycles. The solid line in (a) depicts the theoretical 1:1 line ( ) whilst the dashed lines show ± 40 % (---). In (b), comparisons of profiles of the time and frequency averaged suspended sediment concentration are presented, taken from four 5 minute mean profiles obtained on 23/11/2011 at the times shown.

Figure 10 – Synoptic 2D-HV BASSI images of suspended sediment concentration and bedforms, over a 1.5 m transect in the bottom 0.5 m above the bed, at selected times given in the subplots covering a period of 3.5 s. The colour scale represents the logarithmic value of the concentration. The white arrow in each plot represents the direction and magnitude of the current flow at 0.4 m above the bed. Packets of suspended sediment events and their location over time are identified by A, B and C.

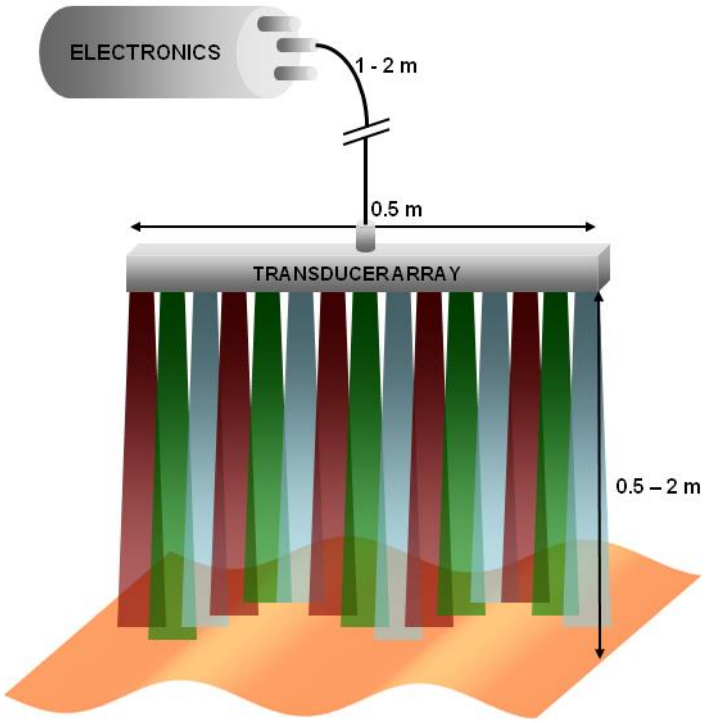

Figure 1 – Schematic of the Bedform And Suspended Sediment Imager, showing one transducer array connected to the electronic scheduling unit, mounted above the seabed. The different coloured beams represent the different operating frequencies of 2.5 MHz (red), 1.25 MHz (green) and 0.75 MHz (blue).

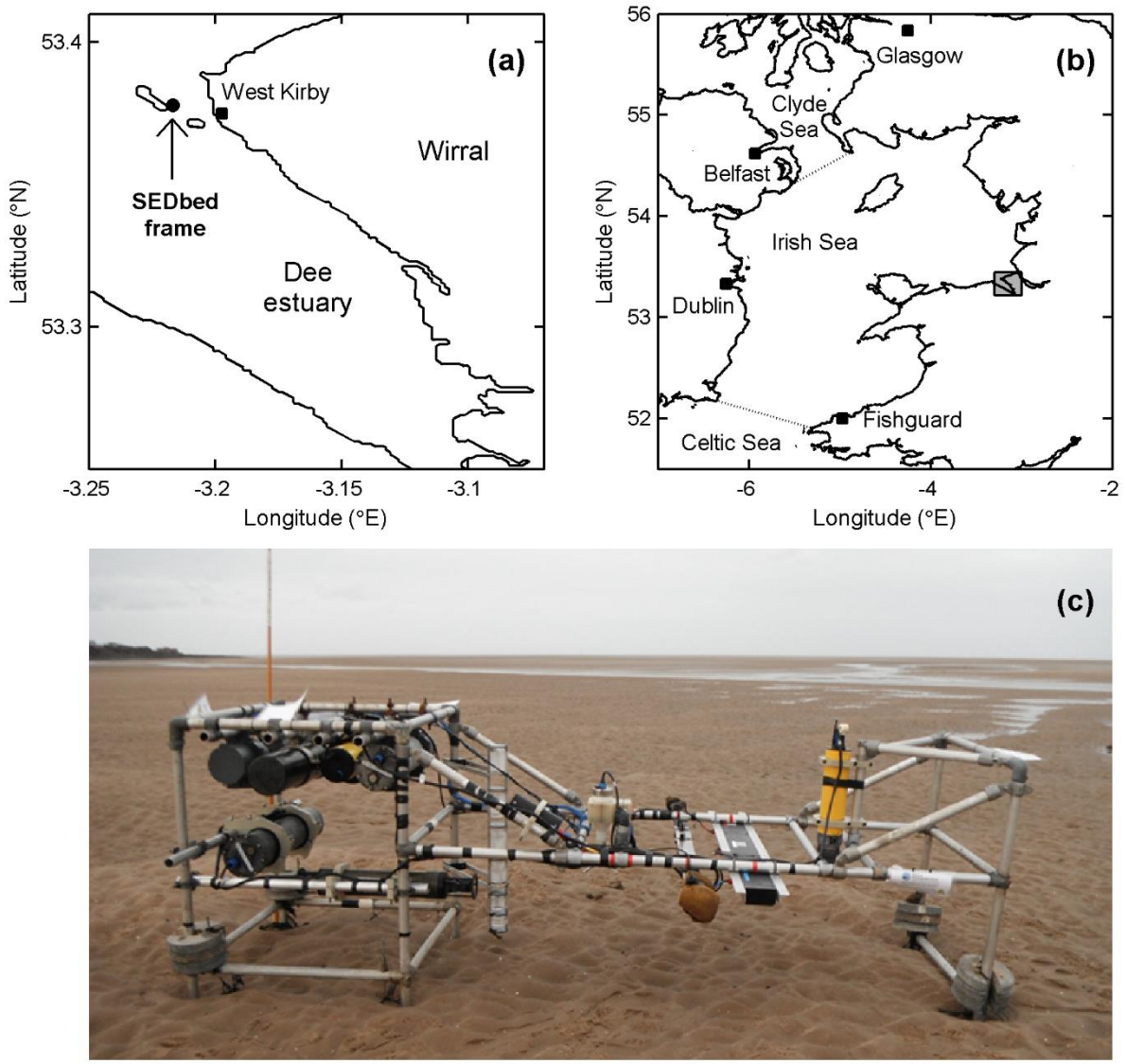

Figure 2 – The study site in the Dee estuary (a), and its location relative to the adjacent Irish Sea (b), as indicated by the shaded box. A photo of the SEDbed instrument frame at low water is shown in (c), looking Northwest towards the Irish Sea. The photo in (c) was taken after two tidal cycles, and illustrates the low impact of the frame on the bed underneath the instrument sensors.

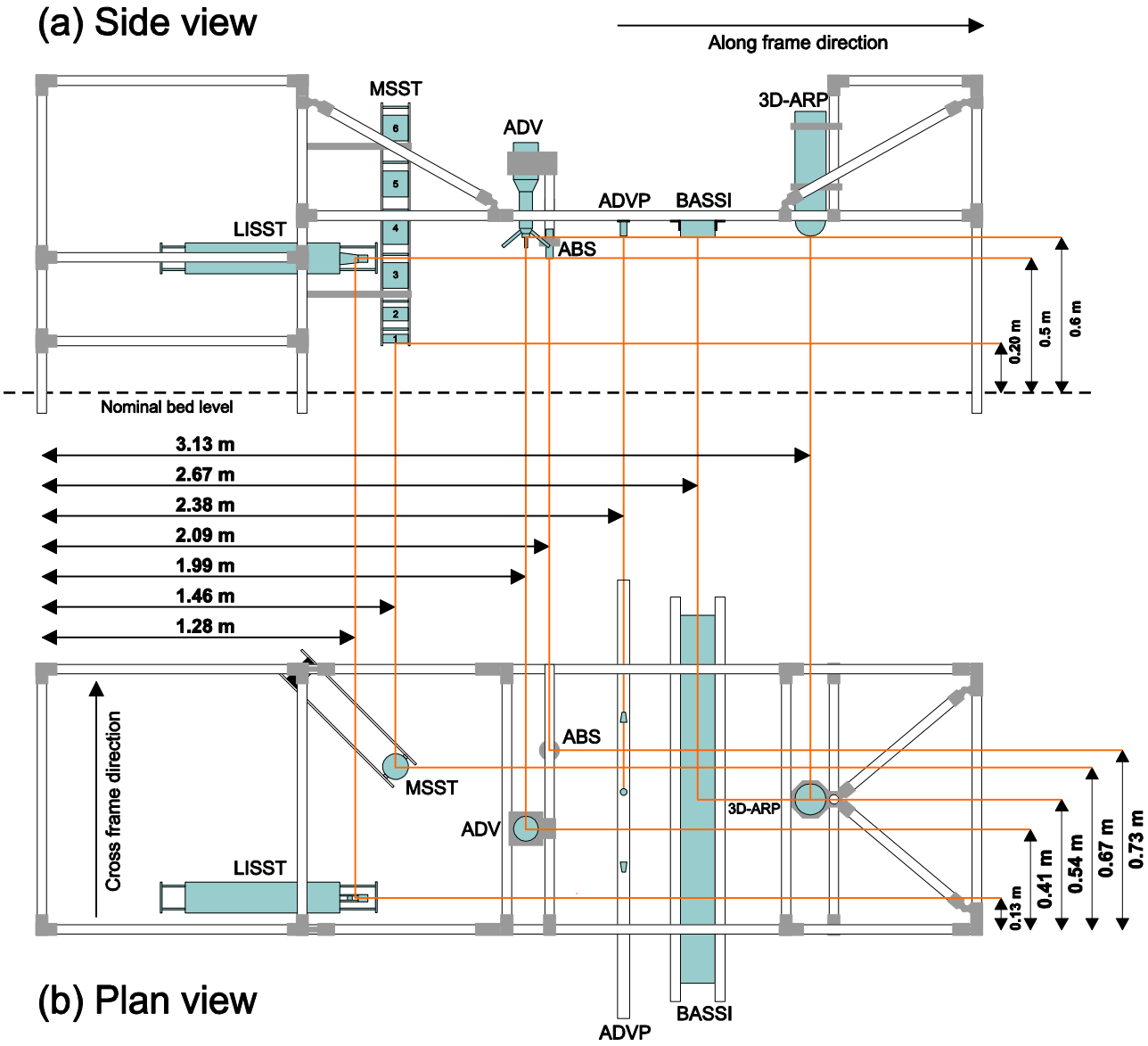

Figure 3 – Schematic of the SEDbed instrument frame, showing the relative location of the Bedform And Suspended Sediment Imager (BASSI), AQUAscat Acoustic Backscatter System (ABS), Acoustic Doppler Velocimeter (ADV), Acoustic Doppler Velocity Profiler (ADVP), three dimensional Acoustic Ripple Profiler (3D-ARP), LISST, and Multi-Stage Sediment Trap (MSST).

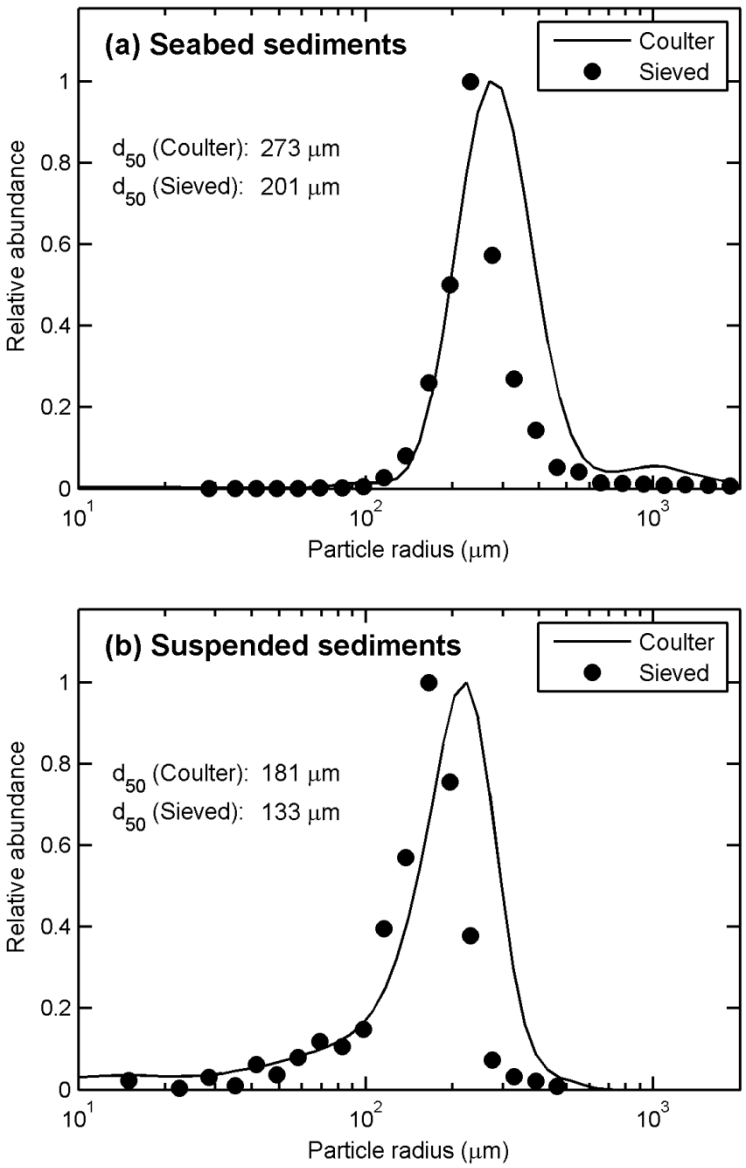

Figure 4 – Particle size distribution spectra obtained from (a) a seabed grab sample, and (b) MSST sediment trap 3 (see Figure 3a), collected on 24/11/2011. The median particle size, d_{50}, obtained from each method is also shown in each plot.

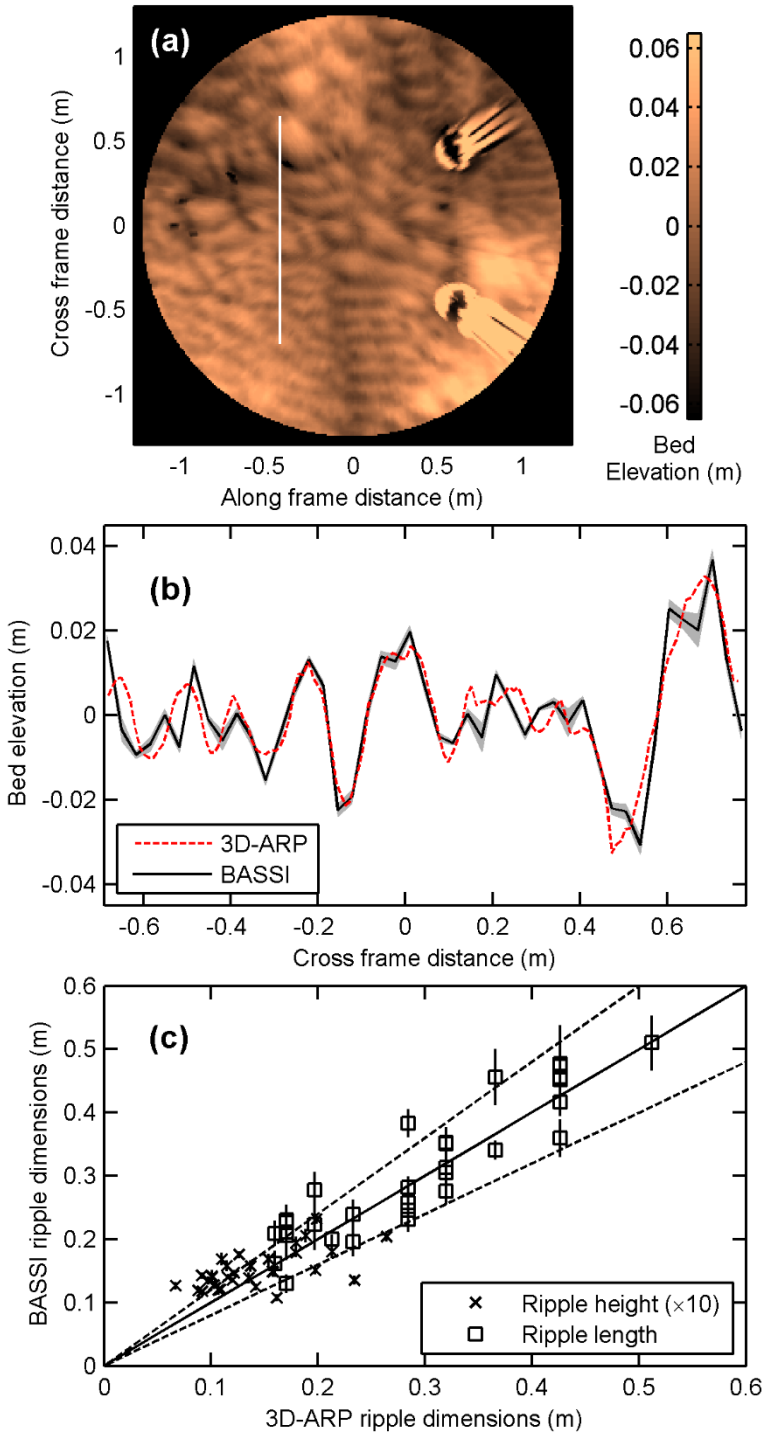

Figure 5 – Ripple measurements obtained from the 3D-ARP and BASSI. A ripple image typical of those observed by the 3D-ARP is shown in (a), along with the location of the BASSI footprint (white solid line). A comparison of the ripple profiles observed by the 3D-ARP and BASSI are shown in (b) for the same burst as shown in (a). The shaded envelope in (b) depicts ± two standard errors about the temporal mean BASSI ripple profile. A comparison of the ripple dimensions observed by both instruments is shown in (c), with both

ripple height (×10) and ripple length presented, and the theoretical 1:1 line also shown (—). The dashed lines (---) shown in (c) illustrate ± 20 % about the 1:1 line.

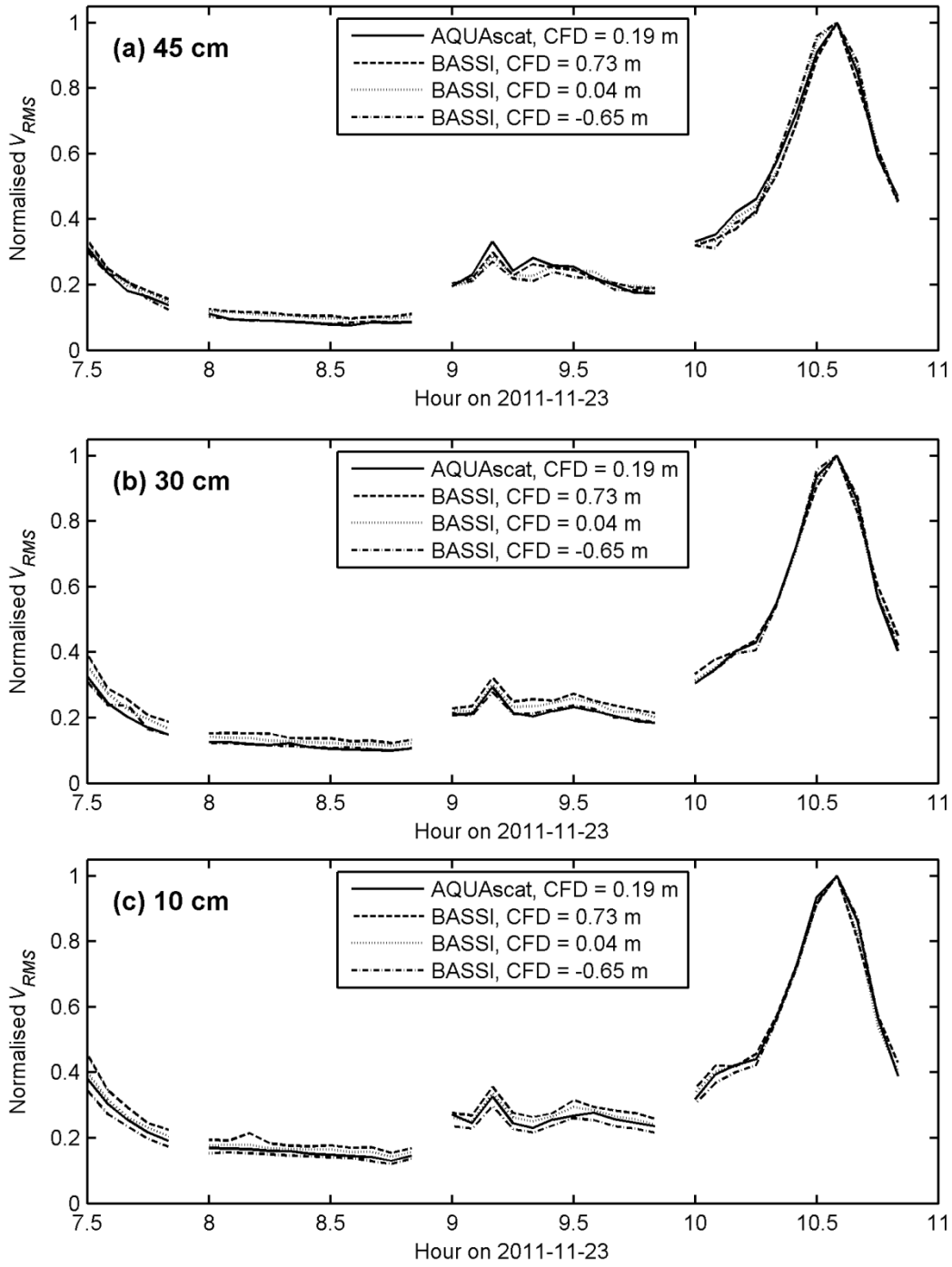

Figure 6 – Normalised V_{RMS} measurements obtained from the AQUAscat and BASSI on 23/11/2011. Measurements are shown at three vertical ranges, being (a) 45 cm, (b) 30 cm, and (c) 10 cm from the AQUAscat transducer. For the tidal cycle shown, high water slack occurred at ~ 08:40. All data shown were obtained at the operating frequency common to both instruments, 2.5 MHz, with data presented from three BASSI transducers located across the 1.5 m array. The cross frame distance (CFD) , relative to the centre of the BASSI array, is shown for each sensor.

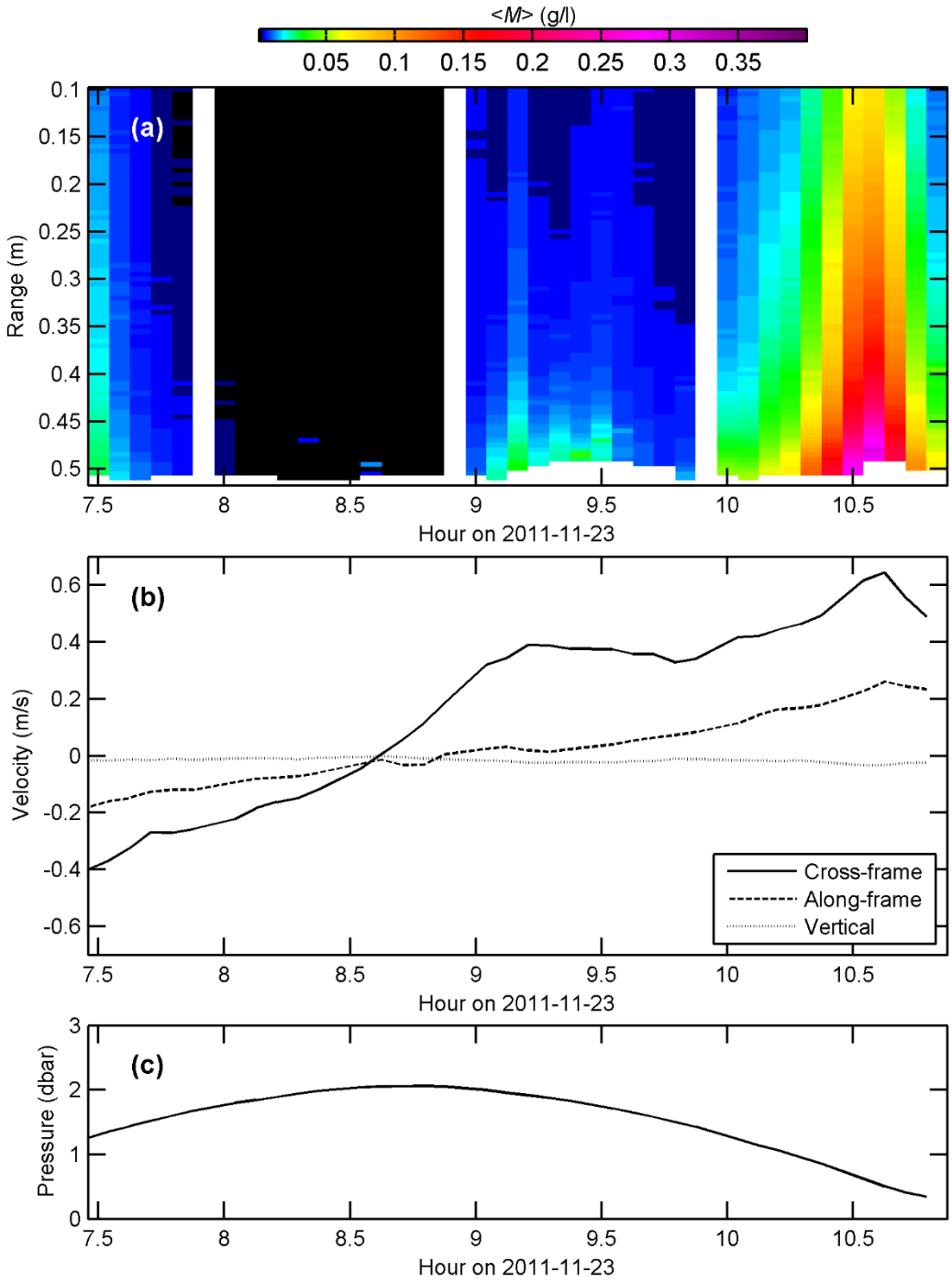

Figure 7 – Time-averaged suspended sediment concentrations, <*M*> (a), ADV velocities (b), and ADV pressure (c), on the morning of 23/11/2011. The sediment concentrations shown in (a) can be seen to be least around high water slack, with increases in <*M*> coinciding with peaks in cross frame velocity seen in (b).

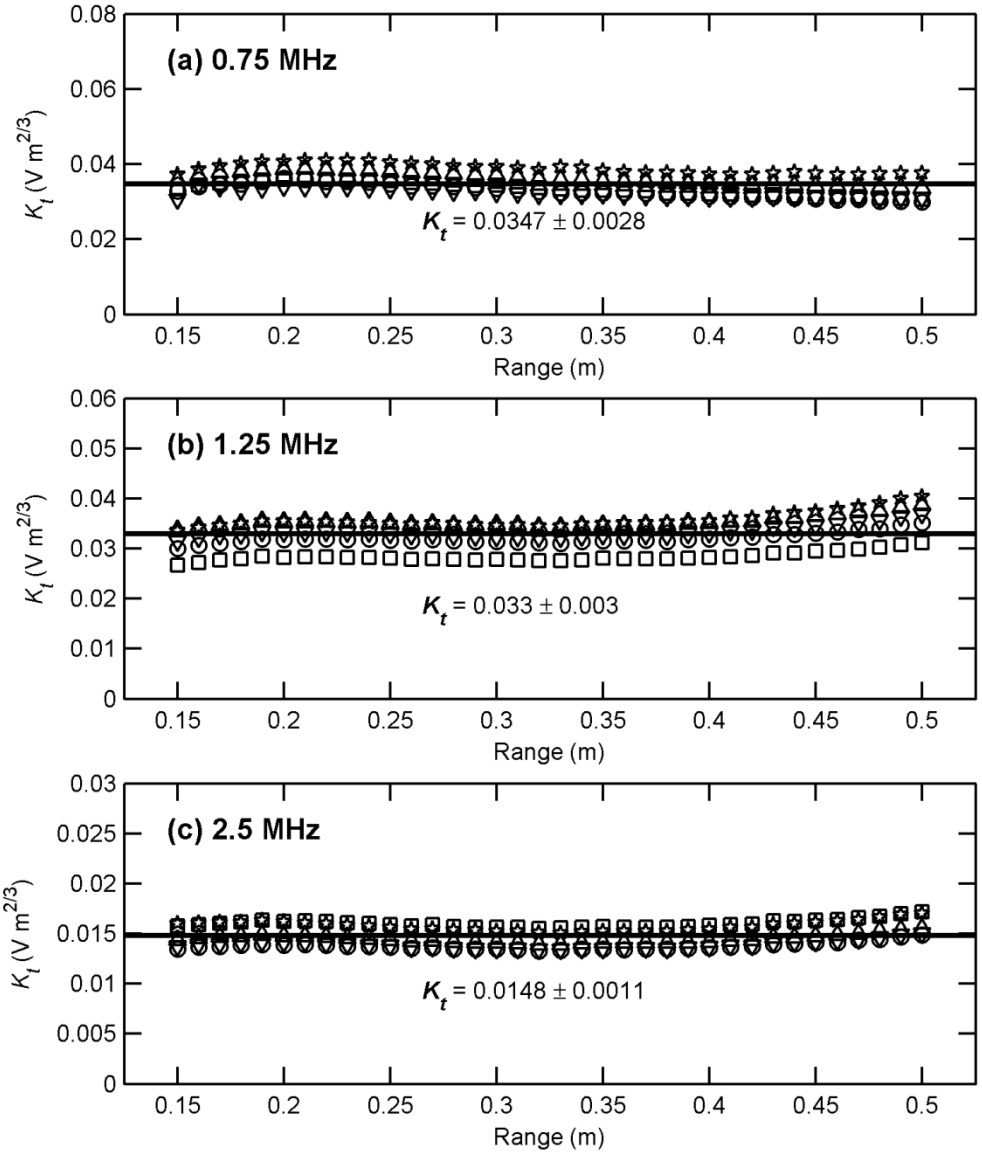

Figure 8 – Profiles of BASSI calibration coefficients, K_t, obtained from the central array. Profiles are shown from each transducer in the array, grouped by operating frequency, with each profile shown being the average of a number of profiles obtained across the four tidal cycles sampled. The overall mean K_t for each operating frequency is also shown (—) and annotated, along with the associated standard deviation.

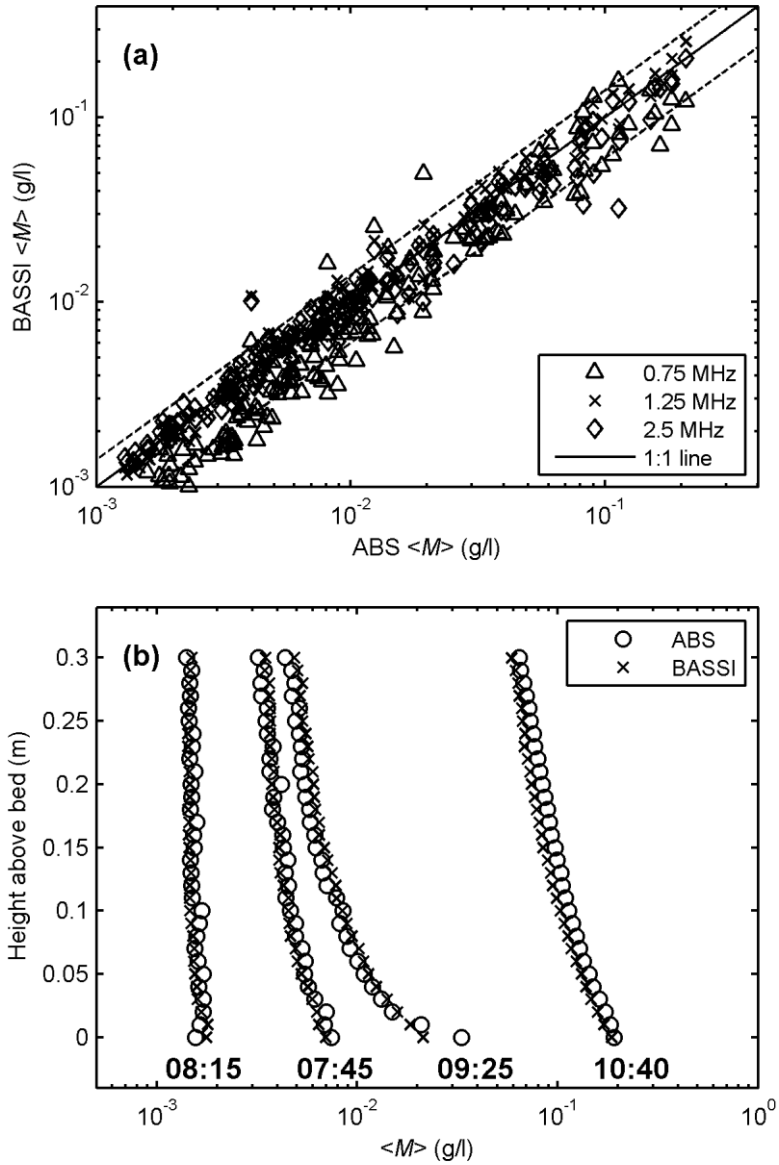

Figure 9 – Comparison of inversion estimates of time-averaged suspended sediment concentration obtained from the BASSI with time-averaged and frequency averaged concentrations obtained from the AQUAscat. In (a), comparisons are shown at a height of 10 cm above the bed for each of the 5 minute mean profiles obtained from each burst from each of the four tidal cycles. The solid line in (a) depicts the theoretical 1:1 line (—) whilst the dashed lines show ± 40 % (---). In (b), comparisons of profiles of time and frequency averaged suspended sediment concentration are presented, taken from four 5 minute mean profiles obtained on 23/11/2012 at the times shown.

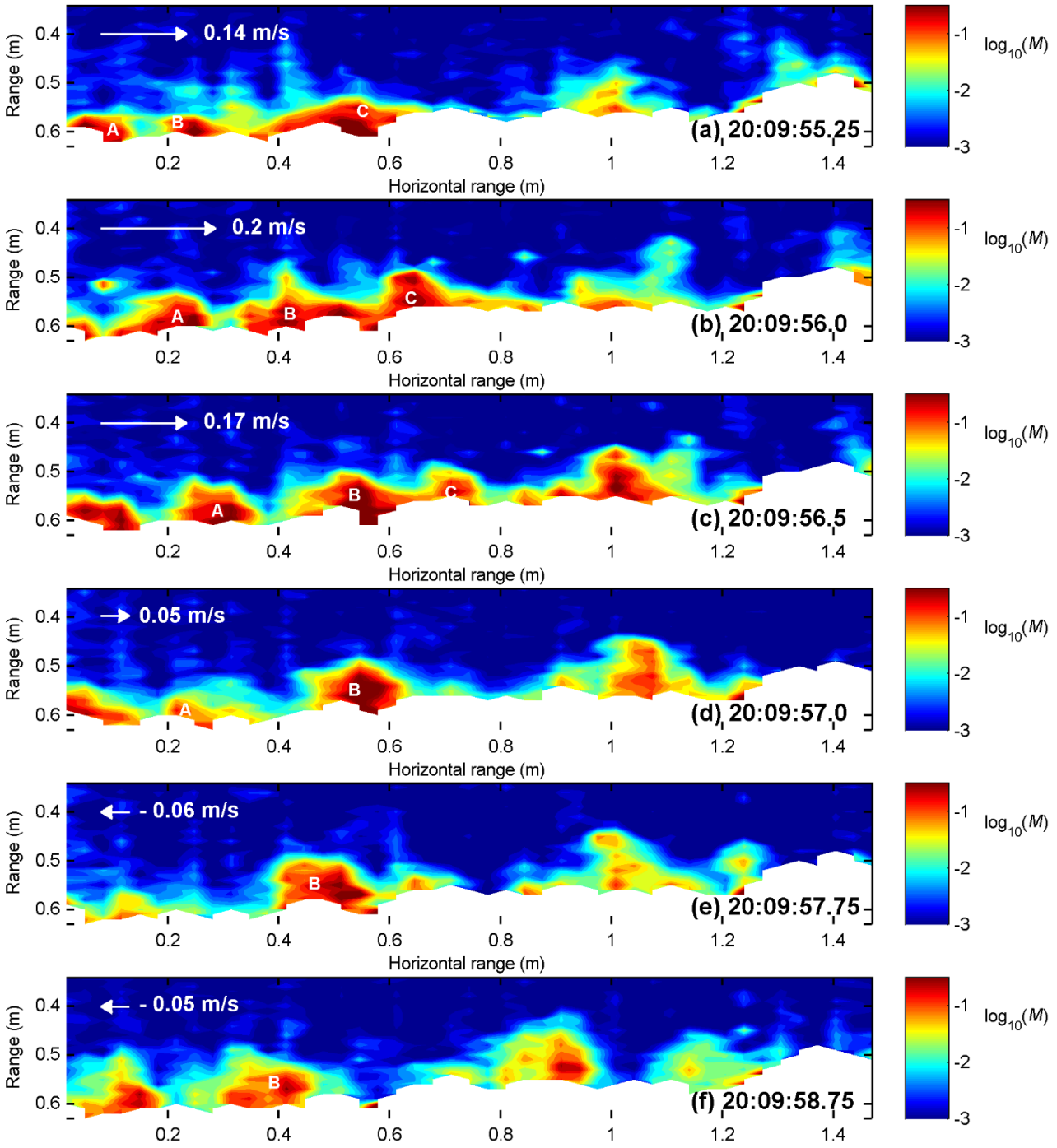

Figure 10 – Synoptic 2D-HV BASSI images of suspended sediment concentration and bedforms, over a 1.5 m transect in the bottom 0.5 m above the bed, at selected times given in the subplots covering a period of 3.5 s. The colour scale represents the logarithmic value of the concentration. The white arrow in each plot represents the direction and magnitude of the current flow at 0.4 m above the bed. Packets of suspended sediment events and their location over time are identified by A, B and C.